Protein Misfolding

International Edition: DOI: 10.1002/anie.201501011
German Edition: DOI: 10.1002/ange.201501011

Structural Effects of Multiple Pathogenic Mutations Suggest a Model for the Initiation of Misfolding of the Prion Protein**

*Jogender Singh and Jayant B. Udgaonkar**

Abstract: *A molecular understanding of the prion diseases requires delineation of the origin of misfolding of the prion protein (PrP). An understanding of how different disease-linked mutations affect the structure and dynamics of native monomeric PrP can provide a clue about how misfolding commences. In this study, hydrogen–deuterium exchange mass spectrometry was used to show that several disease-linked mutant variants, which are thermodynamically destabilized, share a common structural perturbation in their native states: helix 1 is destabilized to an extent that correlates well with the destabilization of the native protein. The mutant variants misfold and form oligomers faster than does the wild-type protein, at rates that increase exponentially with the extent to which helix 1 is destabilized in the native protein. It appears, therefore, that the loss of helix 1 structure marks the beginning of PrP misfolding and oligomerization.*

Prion diseases are incurable and fatal neurodegenerative disorders.[1,2] In humans, the prion diseases include Creutzfeldt–Jakob disease (CJD), Gerstmann–Sträussler–Scheinker syndrome (GSS), and fatal familial insomnia (FFI).[1,2] Prion diseases occur in several other mammalian species as well, and all the prion diseases share a common molecular trait: misfolding of the mainly α-helical, monomeric cellular prion protein (PrP^C) into the mainly β-structured, multimeric PrP^{Sc} (scrapie PrP) form.[1,2] Although the conversion of PrP^C into PrP^{Sc} is linked with prion pathogenesis, the mechanism of this conversion is poorly understood.[3]

Prion diseases can be of sporadic, genetic, or infectious origin.[1] In genetic or familial disease, single nucleotide mutations, which lead to single amino acid changes in PrP, as well as insertions/deletions in the gene encoding PrP, appear to increase the likelihood of neurodegeneration.[1] In humans, many mutations have been linked to familial CJD, GSS, and FFI.[4] Since sporadic occurrence accounts for about 85% of prion diseases, it would appear that spontaneous misfolding of PrP^C into PrP^{Sc} is the major cause of prion diseases. It is likely that familial mutations act by increasing the likelihood of the misfolding of PrP^C into PrP^{Sc}.[5] Studies of the structures and dynamics of disease-linked mutant variants of PrP are expected to help in understanding how misfolding is triggered in native PrP.

Despite the clear involvement of PrP^{Sc} in prion pathogenesis, the composition of PrP^{Sc} is not yet well-known.[3] PrP amyloid fibrils may be toxic and/or infective,[6–8] and there is also evidence suggesting that soluble misfolded oligomeric forms of PrP are toxic and/or infectious.[9–13] Clearly, an understanding of the initial structural changes in monomeric PrP that lead to its misfolding into oligomeric PrP is crucial for understanding prion pathogenesis.

Recombinant PrP forms misfolded oligomers in vitro in a pH-dependent manner. In the presence of 150 mM NaCl but in the absence of chemical denaturants, the amount of misfolded oligomer increases as the pH value decreases, and the pH-induced transition is characterized by an apparent pK_a value of 4.7.[14] Hence, PrP would form oligomers even at physiological pH values but to an undetectable extent. Moreover, since the oligomerization rate is concentration-dependent,[15] the extent of oligomer formation in vivo would also depend upon the local concentration of PrP. Interestingly, aggregation of PrP has been shown to occur in the endocytic pathway,[16] in which lysosomes have a low internal pH value. It is likely that PrP misfolds to oligomeric forms when it encounters low pH values in the endocytic pathway. Importantly, oligomers formed in vitro at low pH values have been shown to be cytotoxic,[17,18] and susceptibility to sporadic prion disease appears to correlate well with the propensity of recombinant PrP to form these oligomers.[19] The oligomers formed at low pH values can disrupt lipid membranes,[14,20] thus pointing towards a putative mechanism for their toxicity. Nevertheless, more research is needed to establish, unequivocally, the relevance of oligomers observed to form in vitro to the disease process in vivo.

To gain insight into the mechanism of PrP misfolding, the structure of the misfolded oligomers formed by recombinant mouse prion protein (moPrP) at pH 4 in the presence of 150 mM NaCl, at 37 °C and at a 100 μM protein concentration was first characterized by hydrogen–deuterium exchange (HDX) measurements coupled with mass spectrometry (MS; HDX-MS). At pH 4 under these conditions, more than 95% of the protein had formed oligomers. In HDX studies, structured regions of the protein are generally protected against HDX, and unstructured, solvent-exposed regions are labeled with deuterium. The labeled segments show an increase in mass and can be identified by carrying out peptic digestion at a low pH value, under which conditions the exchange reaction is quenched. In this way, localized infor-

[*] J. Singh, Prof. J. B. Udgaonkar
National Centre for Biological Sciences
Tata Institute of Fundamental Research
Bengaluru 560065 (India)
E-mail: jayant@ncbs.res.in

[**] This research was funded by the Tata Institute of Fundamental Research and by the Department of Biotechnology, Government of India. We thank members of our research group as well as M. K. Mathew for discussions and comments on the manuscript, and Hitesh Rafalia for help with the CD experiments. J.B.U. is a recipient of a J.C. Bose National Fellowship from the Government of India.

Supporting information for this article is available on the WWW under http://dx.doi.org/10.1002/anie.201501011.

mation about the structural dynamics of different parts of the protein can be obtained. Moreover, since pH 4 is close to the pH value at which intrinsic HDX rates are at their minimum, HDX can be observed at the maximum number of amide hydrogen-atom sites, which are spread over all the secondary structural elements of the protein.

A previously generated peptide map[20] was used for the current study. The oligomers were labeled in D_2O buffer for different time periods, and at different time intervals during labeling an aliquot was withdrawn and mixed with an ice-cold quench buffer (pH 2.5). After desalting, the sample was injected into the HDX module for on-line pepsin digestion at a low pH value. The peptic fragments were then separated and infused into the mass spectrometer to determine their masses. Different regions of wild-type (wt) moPrP were labeled to different extents in the native monomer and in the oligomers (Figure 1 a,b). Helix 2 (α2) and the C-terminal part

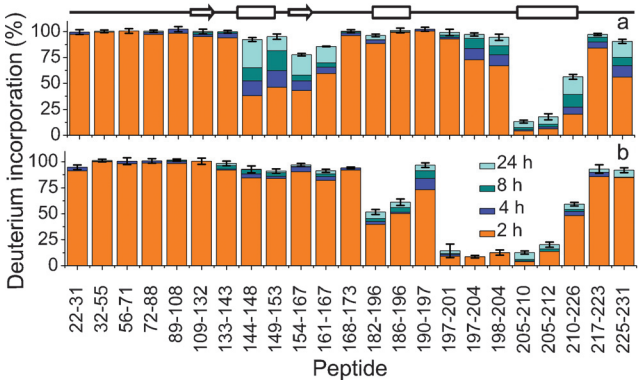

Figure 1. HDX-MS characterization of wt moPrP oligomers formed at pH 4. Deuterium incorporation into different sequence segments of a) monomeric native moPrP and b) oligomers. Stacked bars show the extent of HDX labeling after different time periods as shown in (b). Amino acid residue 22 at the N terminus is Met. The error bars show the standard deviation determined from three independent experiments.

of the loop between α2 and helix 3 (α3) showed higher protection in the oligomers than in the monomer, whereas α3 was protected in both the monomer and oligomers. α3 is one of the most HDX-protected regions in the moPrP monomer.[20,21] Hence, it is difficult to distinguish whether the α3 region retains helicity or is converted into a β sheet in the oligomers. However, since the oligomers formed under the conditions used are known to be β-sheet rich,[14] it is likely that the regions which are HDX-protected in the oligomers are transformed into β sheets. Interestingly, the oligomers formed at pH 4 were observed, in the current study, to have a HDX pattern very similar to those of oligomers that form at pH 2.[20] Moreover, like the oligomers formed at pH 2, the oligomers formed at pH 4 showed bimodal mass distributions with a proportion of protected species of approximately 5% (see Figure S1 in the Supporting Information) for the sequence segments 109–132 and 154–167, thus indicating that these segments are structured in only about 5% of the oligomeric protein population. An HDX study of authentic mouse-brain-derived PrP^{Sc} [22] had indicated that its structural core, encompassing the sequence segment 90–230, was extended as compared to that of the straight amyloid fibrils formed by any recombinant prion protein.[23,24] The current study of oligomers suggests that in at least some (ca. 5%) of the oligomer protein molecules, the structural core may be longer than that of the straight fibrils and about as long as that in PrP^{Sc}.[22] Thus, it appears that the oligomers formed in vitro may be a better model for PrP^{Sc} than fibrils formed under other conditions.

Sequence segment 168–173 does not show any protection against HDX in the oligomers, but sequence segment 182–196 does. In the peptide map of moPrP, the sequence segment 174–181 is missing. Hence, the protected core region for the oligomers might start somewhere in the sequence segment 174–181. At the C-terminal end of the core, the sequence segment 217–223 does not show any protection, but the sequence segment 210–226 shows partial protection, thus indicating that the core region extends up to residue 216. Importantly, the core region is not continuous: the sequence segment 190–197 shows little if any protection (Figure 1 b; see also Figure S2). Hence, this segment is likely to be involved in a turn/loop that divides the core region into two parts.

Importantly, the sequence segments 144–148 and 149–153, which encompass helix 1 (α1), show significantly more deuterium incorporation in the oligomers than in the monomer, thus indicating that α1 is likely to be unfolded in the oligomers (Figure 1; see also Figure S2). Since the structured C-terminal domain of PrP undergoes major structural rearrangement during its misfolding, it is important to dissect the misfolding reaction into individual steps to obtain a molecular understanding of its mechanism.

Several pathogenic mutations are known to destabilize PrP.[25,26] Some of these mutant variants have increased misfolding and oligomerization rates.[27,28] It has been proposed that the pathogenic mutations increase the propensity for the formation of intermediate(s), which might act as the direct precursor(s) to misfolded forms.[26] To gain insight into the effect of destabilization on the misfolding of PrP, and its link with the structural dynamics of PrP, five pathogenic mutant variants of PrP were generated by site-directed mutagenesis: D177N, F197S, D201N, R207H, and Q216R (mouse numbering; mouse numbering is used throughout this Communication; see Figure S3). The identity and purity of these mutant variants were confirmed by mass spectrometry (data not shown).

Denaturant-induced unfolding transitions of D177N, F197S, D201N, R207H and Q216R moPrP, determined under conditions where the proteins are monomeric, show that they are significantly destabilized compared to wt moPrP. The destabilization increases in the order wt < R207H < F197S < D201N < D177N < Q216R (see Figure S4a and Table S1). The midpoints (T_m) of thermally induced unfolding transitions at pH 4 showed a similar trend (see Figure S4b and Table S1).

To understand further how the destabilization of moPrP leads to its misfolding and oligomerization, the kinetics of misfolding and oligomerization of 100 μM moPrP were studied in the presence of 150 mM NaCl at pH 4 and 37 °C. As shown previously,[14] wt moPrP misfolds, as probed by the

change in circular dichroism (CD), and oligomerizes, as probed by size-exclusion chromatography (SEC), to completion within 24 h under these conditions (see Figure S5). The rates of misfolding and oligomerization are identical for wt moPrP (see Figure S5). On the other hand, the mutant variants oligomerized rapidly: most underwent more than 80% oligomerization within 5 min (see Figure S6). The resulting oligomers were misfolded and β-sheet rich (see Figure S7). To quantify the relationship between the misfolding rate and the thermodynamic destabilization, the misfolding kinetics of the mutant variants were probed by CD at 228 nm (Figure 2a). The misfolding kinetics were similar at 216 and 228 nm (see Figure S5d). The mutant variants misfolded rapidly, at rates that increased exponentially with the extent of destabilization (Figure 2b).

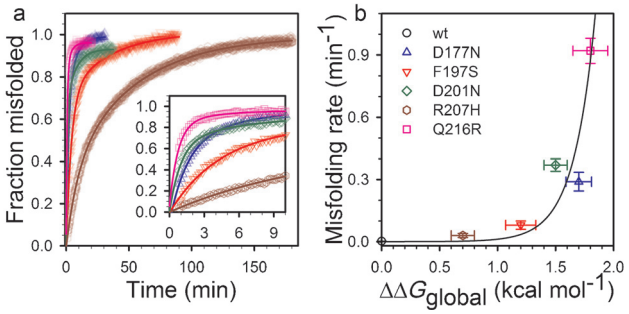

Figure 2. Effect of the pathogenic mutations on the misfolding of moPrP. a) Representative kinetic traces of the misfolding of the different moPrP variants as probed by the change in the CD signal at 228 nm. The inset shows the results for the initial 10 min of misfolding. b) Plot of the mean rate of misfolding against the decrease in stability ($\Delta\Delta G$) with respect to wt moPrP (see Table S1 in the Supporting Information for the $\Delta\Delta G$ values for the different moPrP variants). The continuous lines through the data points in (a) and (b) are fits to exponential equations (see Supporting Information). The symbols and colors for the different moPrP variants are the same in (a) and (b). The error bars show the standard deviation determined from three independent experiments.

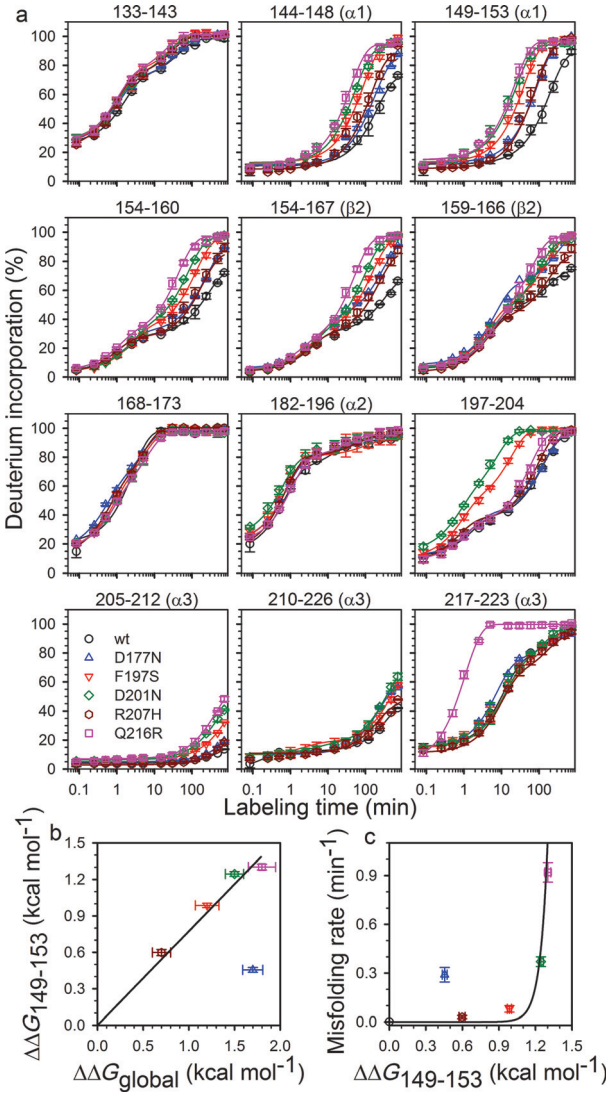

Figure 3. Time course for the labeling of different secondary-structure regions of moPrP variants by HDX at 25 °C and pH 4. a) Percent-deuterium-incorporation profiles of selected sequence segments. The lines through the data points are fits to either a monoexponential or a biexponential equation. b) Comparison of the $\Delta\Delta G$ values calculated from HDX labeling rates for segment 149–153 covering α1 with the global $\Delta\Delta G$ values. The line through the data points is a linear fit to the data points, excluding that of D177N moPrP. c) Plot of the mean rate of misfolding of the different moPrP variants at a 100 μM concentration in 150 mM NaCl at 37 °C and pH 4 against the decrease in stability ($\Delta\Delta G$) of α1. The line through the data points, excluding that of D177N moPrP, is a fit to a single-exponential equation. The symbols and colors for the different moPrP variants are the same in (a–c). The error bars in (a–c) show the standard deviation determined from three independent experiments.

It was important to determine whether the pathogenic mutations altered the structural dynamics of the native state of moPrP in a manner linked to their destabilization. It was also necessary to find out whether the different pathogenic mutations perturbed the structural dynamics of moPrP in a similar manner, since all of them showed drastically increased misfolding rates relative to that of wt moPrP. In particular, if the mutations cause a common structural perturbation, that effect might provide a better understanding of how misfolding commences. To this end, HDX-MS studies were used to probe the structural dynamics in different secondary-structural regions of the pathogenic mutant variants and wt moPrP. HDX into the native proteins was carried out at pH 4 (see above), as the misfolding of the different variant proteins, as initiated by the addition of 150 mM NaCl, was carried out at this pH value.

Most of the mutant variants showed increased rates of deuterium incorporation in the vicinity of the site of the mutation (Figure 3a). F197S and D201N moPrP showed increased rates of deuterium incorporation into the sequence segment 197–204, and Q216R moPrP showed increased rates of deuterium incorporation into the sequence segment 217–223. Owing to the change in mass because of the mutation, the sequence segment 210–226 of Q216R moPrP could not be distinguished from another peak at the same m/z value, and hence could not be analyzed. However, the increased deuterium-incorporation rate in the sequence segment 217–

223 shows that Q216R moPrP has increased structural dynamics in the vicinity of the mutation site. Because of the gap in the peptide map in the region 174–181, the local effect in D177N moPrP could not be studied. R207H moPrP did not show any change in the deuterium-incorporation rates in the sequence segments in the vicinity of the mutation site (Figure 3a).

Besides causing local perturbations in the deuterium-incorporation profiles, the destabilizing pathogenic mutations cause a common structural perturbation: the sequence segments covering α1 and the loop between α1 and β-strand 2 (β2) show increased structural dynamics, as indicated by increased rates of deuterium incorporation into these regions (Figure 3a). The HDX rates were used to calculate the thermodynamic stability of the sequence segment 149–153, which represents α1 (see the Supporting Information). Importantly, the local destabilization increases in the order: D177N ≈ R207H < F197S < D201N < Q216R. More importantly, excluding D177N moPrP, the local $\Delta\Delta G$ values correlate well with the global $\Delta\Delta G$ values: a plot of local $\Delta\Delta G$ versus global $\Delta\Delta G$ has a slope of 0.8 (Figure 3b). Although D177N moPrP shows reduced stability in the α1 region, the reduction in its global stability does not correlate well with the reduction in α1 stability, most likely because local destabilizing effects dominate in D177N. The mean misfolding rate of moPrP increases exponentially with the extent of destabilization of α1 (Figure 3c). It appears that the decrease in the stability of α1 is primarily responsible for the decrease in stability of the different pathogenic mutant variants and has a strong effect on moPrP misfolding.

In a previous study,[14] it had been shown that stabilization of the C terminus of α2 by mutation of the sequence stretch TVTTTT to AAAAAA prevented the resultant mutant moPrP (A6 moPrP) from misfolding and oligomerization. This study suggested that the conformational conversion of α2 and α3 into β structure in the oligomers (Figure 1; see also Figure S2) occurs as the defining step in oligomerization, but could not identify any earlier structural perturbation in the monomer that might facilitate the conformational conversion of α2 and α3. The current study suggests that this earlier structural perturbation could be increased structural dynamics in α1. To probe the sequence of these structural changes, we created the D201N mutation in A6 moPrP to obtain D201N-A6 moPrP, in which α1 is expected to be destabilized and α2 is expected to be stabilized as compared to α1 and α2 in wt moPrP, respectively. Indeed, as found for D201N, D201N-A6 moPrP showed increased rates of deuterium incorporation into α1 and in the vicinity of the mutation site (see Figure S8). D201N-A6 moPrP also showed increased stability of α2, as has been seen for A6 moPrP.[14] However, unlike D201N-A6 moPrP and like wt moPrP, A6 moPrP did not show any change in the stability of α1.[14] As expected, D201N-A6 moPrP showed increased thermodynamic stability as compared to D201N moPrP (see Figure S9a). Importantly, D201N-A6 moPrP did not show any oligomer formation even in 5 days in the presence of 150 mM NaCl at pH 4 and 37 °C and at a 100 μM protein concentration (see Figure S9b), whereas D201N moPrP misfolded and oligomerized completely within 1 h (Figure 2a; see also Figure S6). The D201N-A6 moPrP monomer remained completely helical under the above misfolding conditions (see Figure S9c).

The results suggest a working model for the initiation of the misfolding and oligomerization of moPrP (Figure 4). The model posits an unraveling of helix 1 in the first step. Since amide hydrogen atoms are usually protected by hydrogen bonding,[29] this conformational change would lead to the significantly higher exchange rate observed for this region in HDX-MS studies of the native states of the different pathogenic mutant variants. It is also possible that the increased structural dynamics observed for this region may be a consequence of the movement of α1 away from α2 and α3 and thus greater solvent exposure of the amide hydrogen atoms in α1. The exact nature of the structural perturbation that leads to a lowering of the protection against HDX of the amide hydrogen atoms of α1 remains to be ascertained. All mutations studied have either a direct or an indirect link with α1 or the flanking regions, including mainly the loop between α1 and β2 (see Figure S3). It is likely that any perturbation, whether a mutation or any chemical perturbation which destabilizes the interactions between α1 and α2–α3, would lead to increased misfolding of PrP. Indeed, a reduction in the pH value has been shown to lead to a reduction in the tertiary contacts between α1 and α3 in the pathogenic mutant variant V210I.[30] In the second step of the model, once α1 has lost structure, the high intrinsic propensity of α2 to form a β sheet and/or random coil[31] would lead to the misfolding of α2 and α3 (Figure 4). Interestingly, the isolated sequence segment comprising only α2–α3 forms oligomers faster than does full-length PrP,[32] thus suggesting that the lack of interactions with α1 in isolated α2–α3 leads to faster oligomerization. Parts of α2 and α3 form the structural core of the oligomers, whereas α1 appears to be unfolded in the oligomers (Figures 1 and 4; see also Figure S2). Recently, it was shown that a reduction in the pH value leads to the formation of a molten-globule form of PrP in which the β1–α1–β2 subdomain has reduced structure.[33] This transformation is similar to the first step of the mechanism shown in Figure 4. This molten globule is likely to act as a direct precursor to the misfolded oligomer. It

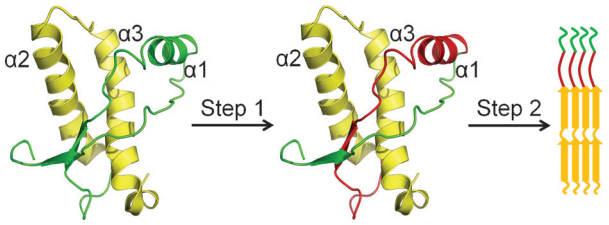

Figure 4. Model for the molecular mechanism of moPrP misfolding and oligomerization. Misfolding in native PrP may commence by the loss of structure in α1 and the loop between α1 and β2. The increased structural dynamics in α1 and the loop between α1 and β2 after step 1 is shown by the change in color from green to dark red. The intrinsic propensity of α2 to convert into a β sheet/random coil then drives the conversion of α2 and α3 into a β sheet. Misfolded oligomers have parts of the α2–α3 region, shown in yellow, converted into a β-sheet core region interrupted by a turn/loop. In the oligomers, α1 is unfolded, as are β1 and β2 (Figure 1; see also Figure S2).

appears then that a reduction in the pH value leads to oligomer formation by the same mechanism used by pathogenic mutant variants, thus pointing towards a common molecular mechanism for the misfolding of PrP.

Such a mechanism for the initiation of moPrP misfolding is supported by the results of earlier studies. Sub-domain separation, of β1–α1–β2 from α2–α3, has been shown to be critical for oligomerization: locking these two sub-domains by disulfide linkage prevents oligomerization.[34] Some computational studies carried out on either wt PrP or pathogenic mutant variants revealed increased structural dynamics in α1 because of the movement of α1 away from α2–α3.[35,36] The antibody ICSM 18, which is known to bind to both α1 and parts of α3,[37] has one of the highest therapeutic potencies for PrP, presumably because it locks PrP and prevents its subdomain separation. Molecules that stabilize the C terminus of α2 have also proved to be effective antiprion drugs, both ex vivo and in vivo,[38] and most likely act by inhibiting step 2 of PrP misfolding. Hence, the current study indicates that the inhibition of either step 1 or step 2 of PrP misfolding by the use of chemical chaperones or drugs would have therapeutic value.

Keywords: hydrogen–deuterium exchange · mass spectrometry · misfolding · pathogenic mutations · prion proteins

How to cite: *Angew. Chem. Int. Ed.* **2015**, *54*, 7529–7533
Angew. Chem. **2015**, *127*, 7639–7643

[1] S. B. Prusiner, *Proc. Natl. Acad. Sci. USA* **1998**, *95*, 13363.
[2] J. Collinge, *Annu. Rev. Neurosci.* **2001**, *24*, 519.
[3] R. Diaz-Espinoza, C. Soto, *Nat. Struct. Mol. Biol.* **2012**, *19*, 370.
[4] M. W. van der Kamp, V. Daggett, *Protein Eng. Des. Sel.* **2009**, *22*, 461.
[5] W. S. Jackson, A. W. Borkowski, H. Faas, A. D. Steele, O. D. King, N. Watson, A. Jasanoff, S. Lindquist, *Neuron* **2009**, *63*, 438.
[6] V. Novitskaya, O. V. Bocharova, I. Bronstein, I. V. Baskakov, *J. Biol. Chem.* **2006**, *281*, 13828.
[7] G. Mallucci, A. Dickinson, J. Linehan, P. Klohn, S. Brandner, J. Collinge, *Science* **2003**, *302*, 871.
[8] P. Piccardo, J. C. Manson, D. King, B. Ghetti, R. M. Barron, *Proc. Natl. Acad. Sci. USA* **2007**, *104*, 4712.
[9] J. R. Silveira, G. J. Raymond, A. G. Hughson, R. E. Race, V. L. Sim, S. F. Hayes, B. Caughey, *Nature* **2005**, *437*, 257.
[10] S. Simoneau, H. Rezaei, N. Salès, G. Kaiser-Schulz, M. Lefebvre-Roque, C. Vidal, J. G. Fournier, J. Comte, F. Wopfner, J. Grosclaude, H. Schätzl, C. I. Lasmézas, *PLoS Pathog.* **2007**, *3*, e125.
[11] P. Tixador, L. Herzog, F. Reine, E. Jaumain, J. Chapuis, A. Le Dur, H. Laude, V. Béringue, *PLoS Pathog.* **2010**, *6*, e1000859.
[12] Y. P. Choi, A. Gröner, J. W. Ironside, M. W. Head, *Brain Pathol.* **2011**, *21*, 298.
[13] Z. E. Anaya, J. Savistchenko, V. Massonneau, C. Lacroux, O. Andreoletti, D. Vilette, *J. Biol. Chem.* **2011**, *286*, 8141.
[14] J. Singh, H. Kumar, A. T. Sabareesan, J. B. Udgaonkar, *J. Am. Chem. Soc.* **2014**, *136*, 16704.
[15] F. Sokolowski, A. J. Modler, R. Masuch, D. Zirwer, M. Baier, G. Lutsch, D. A. Moss, K. Gast, D. Naumann, *J. Biol. Chem.* **2003**, *278*, 40481.
[16] J. E. Arnold, C. Tipler, L. Laszlo, J. Hope, M. Landon, R. J. Mayer, *J. Pathol.* **1995**, *176*, 403.
[17] M. Kristiansen, P. Deriziotis, D. E. Dimcheff, G. S. Jackson, H. Ovaa, H. Naumann, A. R. Clarke, F. W. van Leeuwen, V. Menéndez-Benito, V. N. P. Dantuma, J. L. Portis, J. Collinge, S. J. Tabrizi, *Mol. Cell* **2007**, *26*, 175.
[18] N. Sanghera, M. Wall, C. Vénien-Bryan, T. J. Pinheiro, *Biochim. Biophys. Acta Proteins Proteomics* **2008**, *1784*, 873.
[19] M. Q. Khan, B. Sweeting, V. K. Mulligan, P. E. Arslan, N. R. Cashman, E. F. Pai, A. Chakrabartty, *Proc. Natl. Acad. Sci. USA* **2010**, *107*, 19808.
[20] J. Singh, A. T. Sabareesan, M. K. Mathew, J. B. Udgaonkar, *J. Mol. Biol.* **2012**, *423*, 217.
[21] J. Singh, J. B. Udgaonkar, *J. Mol. Biol.* **2013**, *425*, 3510.
[22] V. Smirnovas, G. S. Baron, D. K. Offerdahl, G. J. Raymond, B. Caughey, W. K. Surewicz, *Nat. Struct. Mol. Biol.* **2011**, *18*, 504.
[23] X. Lu, P. L. Wintrode, W. K. Surewicz, *Proc. Natl. Acad. Sci. USA* **2007**, *104*, 1510.
[24] N. J. Cobb, F. D. Sonnichsen, H. McHaourab, W. K. Surewicz, *Proc. Natl. Acad. Sci. USA* **2007**, *104*, 18946.
[25] S. Liemann, R. Glockshuber, *Biochemistry* **1999**, *38*, 3258.
[26] A. C. Apetri, K. Surewicz, W. K. Surewicz, *J. Biol. Chem.* **2004**, *279*, 18008.
[27] D. L. Vanik, W. K. Surewicz, *J. Biol. Chem.* **2002**, *277*, 49065.
[28] A. C. Apetri, D. L. Vanik, W. K. Surewicz, *Biochemistry* **2005**, *44*, 15880.
[29] H. Maity, W. K. Lim, J. N. Rumbley, S. W. Englander, *Protein Sci.* **2003**, *12*, 153.
[30] I. Biljan, G. Ilc, G. Giachin, J. Plavec, G. Legname, *Biochemistry* **2012**, *51*, 7465.
[31] R. I. Dima, D. Thirumalai, *Biophys. J.* **2002**, *83*, 1268.
[32] N. Chakroun, S. Prigent, C. A. Dreiss, S. Noinville, C. Chapuis, F. Fraternali, H. Rezaei, *FASEB J.* **2010**, *24*, 3222.
[33] R. P. Honda, K. Yamaguchi, K. Kuwata, *J. Biol. Chem.* **2014**, *289*, 30355.
[34] F. Eghiaian, T. Daubenfeld, Y. Quenet, M. van Audenhaege, A. P. Bouin, G. van der Rest, J. Grosclaude, H. Rezaei, *Proc. Natl. Acad. Sci. USA* **2007**, *104*, 7414.
[35] A. De Simone, A. Zagari, P. Derreumaux, *Biophys. J.* **2007**, *93*, 1284.
[36] E. Behmard, P. Abdolmaleki, E. B. Asadabadi, S. Jahandideh, *J. Biomol. Struct. Dyn.* **2011**, *29*, 379.
[37] S. V. Antonyuk, C. R. Trevitt, R. W. Strange, G. S. Jackson, D. Sangar, M. Batchelor, S. Cooper, C. Fraser, S. Jones, T. Georgiou, A. Khalili-Shirazi, A. R. Clarke, S. S. Hasnain, J. Collinge, *Proc. Natl. Acad. Sci. USA* **2009**, *106*, 2554.
[38] Y. O. Kamatari, Y. Hayano, K. I. Yamaguchi, J. Hosokawa-Muto, K. Kuwata, *Protein Sci.* **2013**, *22*, 22.

Received: February 3, 2015
Revised: April 17, 2015
Published online: May 8, 2015

